ELSEVIER
Nuclear Instruments and Methods in Physics Research B 164–165 (2000) 168–179
NIM B
Beam Interactions with Materials & Atoms
www.elsevier.nl/locate/nimb

Slowing down of relativistic few-electron heavy ions

H. Weick [a,b,*], H. Geissel [a,b], C. Scheidenberger [a], F. Attallah [a], T. Baumann [a], D. Cortina [a], M. Hausmann [a], B. Lommel [a], G. Münzenberg [a], N. Nankov [b], F. Nickel [a], T. Radon [a], H. Schatz [a], K. Schmidt [a], J. Stadlmann [b], K. Sümmerer [a], M. Winkler [a], H. Wollnik [b]

[a] *Gesellschaft für Schwerionenforschung, 64291 Darmstadt, Germany*
[b] *II. Physikalisches Institut, Universität Gießen, 35392 Gießen, Germany*

Abstract

Experimental data on energy loss and energy-loss straggling of fully ionized relativistic heavy ions agree well with the theory of Lindhard and Sørensen (LS). However, when heavy ions penetrate matter with many fluctuating ionic charge states the theoretical description is more complicate and less accurate. A novel exploratory step to contribute to a better understanding of the slowing down of heavy ions has been done with the present experiment in an energy region where the atomic interaction is still dominated by bare and few-electron projectiles. In the energy range of 100–1000 MeV/u we measured with the high-resolution magnetic spectrometer FRS the stopping powers, the energy-loss straggling and the charge-state distributions of ^{197}Au, ^{208}Pb and ^{209}Bi projectiles in charge-state equilibrium interacting with solids ranging from beryllium to lead targets. Additionally, charge exchange cross-sections have been measured to support a better analysis and interpretation of the energy-loss data. The experimental results on stopping power and energy-loss straggling clearly demonstrate the contribution of ions in different charge states. A novel application of the slowing down of relativistic exotic heavy ions is presented.

PACS: 34.50.Bw; 34.50.−s; 34.70.+e

1. Introduction

The study of the interaction of heavy ions penetrating matter has received new impacts by the operation of powerful particle accelerators, storage rings, and the developments of new applications. Many review articles have been published, e.g., [1–3], but an accurate description based on first principles has not been achieved for the many body collision processes involving excitation and charge changing of both the target and the projectile atoms. At low energies of a few MeV/u the heavy ion–target interaction is characterized by frequent charge-changing collisions and a rather broad charge-state distribution (CSD), e.g., a uranium projectile still carries about

* Corresponding author. Part of PhD Thesis, Universität Gießen.
E-mail address: h.weick@gsi.de (H. Weick).

0168-583X/00/$ - see front matter
PII: S0168-583X(99)01025-3

40 electrons during its travel through matter. An effective method to reduce the complexity of the atomic heavy-ion interaction are studies at relativistic energies where the projectiles are bare or carry only few electrons. In previous experiments we mainly focused on the interaction of bare projectiles penetrating matter [4,5]. In this case, the experimental results on stopping power and energy-loss straggling are in excellent agreement with the theory of Lindhard and Sørensen (LS) [6].

In this contribution we present new experiments with ^{197}Au, ^{208}Pb and ^{209}Bi projectiles extended down to lower energies to study the onset of the interaction in several, but well defined, charge states. The selected energy range of 100–1000 MeV/u for the projectiles is well suited to investigate the contribution of charge-changing collisions in light and heavy target materials characterized by different mean free path lengths for charge-changing collisions. It should be noted that these path lengths have macroscopic dimensions in solids contrary to low energies, i.e, at relativistic energies the target thickness of solids, a few 100 μg/cm^2, can be easily handled to fulfill the single-collision condition for charge-changing cross-section measurements. Modern applications of the slowing down of relativistic heavy ions are for example tumor treatment [7] and monoisotopic separation of relativistic exotic nuclei [8]. A new application of energy bunching and heavy-ion stopping is also presented in this contribution.

2. Experimental

The combination of the linear accelerator UNILAC and the synchrotron SIS [9] at GSI provides projectile beams of all elements up to uranium with a maximum magnetic rigidity (Bρ) of 18 Tm corresponding to 1.9 GeV/u for ions with a mass-to-charge ratio of two, i.e., the projectiles can reach a maximum velocity of 95% of the speed of light. The projectiles are injected from the UNILAC into SIS at 11.4 MeV/u after passing two stripper sections, and are then accelerated further. There is no stripper target inside SIS. Therefore, the ionic charges of the beams extracted from SIS are generally smaller than the equilibrium CSD would provide at the exit velocity. This special feature is relevant and has to be taken into account in our atomic collision experiments. The projectiles have a momentum spread of about 5×10^{-4} and their transverse emittance is about 1π mm mrad for a low intensity beam of a few thousand ions per second. The absolute energy of the SIS beam, determined by Schottky frequency measurements of the circulating beam, is known with an accuracy of better than 10^{-3}. It should be noted that recently an electron cooler was installed in the synchrotron which can further improve the beam quality for future experiments [10].

The projectile beam is transferred from SIS to the projectile fragment separator FRS [11] shown schematically in Fig. 1. The FRS is a high-reso-

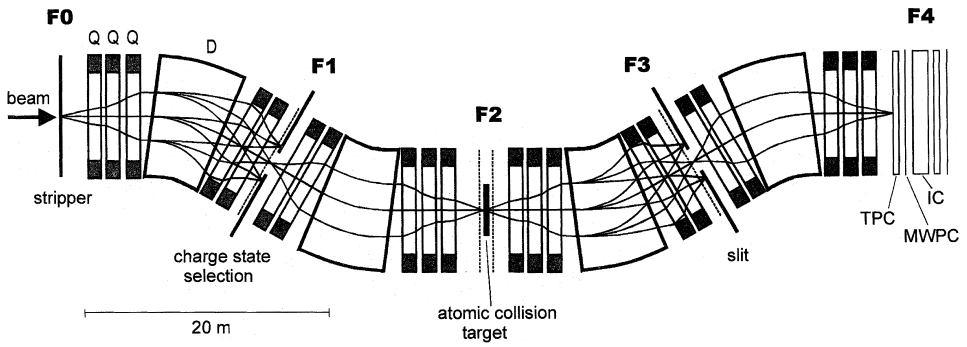

Fig. 1. Scheme of the experimental setup for charge-state and energy-loss experiments at the projectile fragment separator FRS. The ion-optical elements of the FRS (the dipole and quadrupole magnets are indicated by *D* and *Q*, respectively, whereas the hexapole magnets positioned directly in front and behind the dipoles are not shown here). The envelopes of a projectile beam in three different charge states, and the position sensitive detectors (MWPC, TPC) with the ionization chamber (IC) are illustrated. The removable detectors are represented by dashed lines in the scheme.

lution magnetic spectrometer consisting of four dipole stages, each of 18 m length, with altogether 20 quadrupole and 8 sextupole magnets. The maximum magnetic rigidity $B\rho = 18$ Tm is adapted to that of the synchrotron. The dispersive focal planes (F_1)–(F_4) after each dipole stage are equipped with position-sensitive detectors to measure the momentum by magnetic rigidity analysis with an accuracy of better than 5×10^{-4}. The movable detectors at F_1–F_3 are in the vacuum system and can be operated by remote control. At the entrance of the FRS (F_0) a charge-exchange target was optionally positioned to prepare and select the charge state of the ions before they impinge on the atomic-interaction target placed in the central focal plane F_2 of the FRS. The CSD of the ions emerging from the latter target was measured at the third focus F_3 characterized by a $B\rho$ dispersion of 2.2 m. Precise momentum measurements, independent of possible energy fluctuations of the incident beam, were performed via position measurements at the final focal plane F_4 characterized by a dispersion of 8.4 m with respect to the central focus. The total ion-optical system of the FRS is achromatic from the entrance to the final focal plane, i.e., in this mode the FRS is operated as an energy-loss spectrometer. Multi-wire proportional counters (MWPC) and time-projection chambers (TPC) [12] were used for position measurements in two dimensions. The combination of two such detectors, e.g., at the final focal plane allows a complete particle tracking in angle and space. Additionally, an ionization chamber (IC) [13] recorded the energy deposition of the ions to yield particle identification as an indication for possible nuclear reactions. The latter information is only necessary if very thick slowing-down targets are used.

2.1. Charge states

Charge-changing cross-sections (CCCS) and CSD have been measured with position-sensitive detectors at the dispersive focal planes F_3 and F_4 of the FRS, see Fig. 1. For these measurements it is important that the efficiency of the detectors is determined over the complete active area. The targets for CCCS measurements were in the thickness range of 0.01–0.1 mg/cm^2, sufficiently thin to allow for single collision conditions. These self-supporting foils were produced by evaporation and the accuracy of their thickness determination was about 5%. The solid targets for CSD experiments were thicker, in the range of 100–4000 mg/cm^2, and permit a thickness determination with an accuracy of a few mg/cm^2. Measured equilibrium CSD of ^{209}Bi projectiles in lead at 159 MeV/u and 950 MeV/u are presented in Fig. 2 to illustrate the different number of charge states involved in the energy range of the present experiments. The spectra clearly demonstrate the high ion-optical resolution and the low background contribution in the measurements. The relative fraction of each single charge state is indicated.

2.2. Stopping powers

Stopping-power experiments in transmission geometry require both precise energy measurement and target thickness determination. The most probable energy loss was determined by the described position measurements at F_4. The conversion from position spectra to energy distributions implied a careful dispersion calibration at the position in the focal plane where the optical image condition is fulfilled, i.e., the position coordinate is independent of the angles of the projectiles emerging from the target (first-order optical condition). The energy-loss determination had an accuracy of about 5×10^{-3}.

We have measured the stopping power in different solid materials characterized by their atomic number Z_2. Be, Al, Cu, Ag, Ta, Au and Pb in a thickness range 100–4000 mg/cm^2 were used. For a selected incident projectile energy up to four different target thicknesses were used for each Z_2. The stopping power was derived by numerical differentiation using the energy-loss measurements in these different targets. The target materials of very high chemical purity (99.999%) were commercially available, whereas the preparation and thickness determination were performed in the GSI target laboratory [14]. An exception were the beryllium

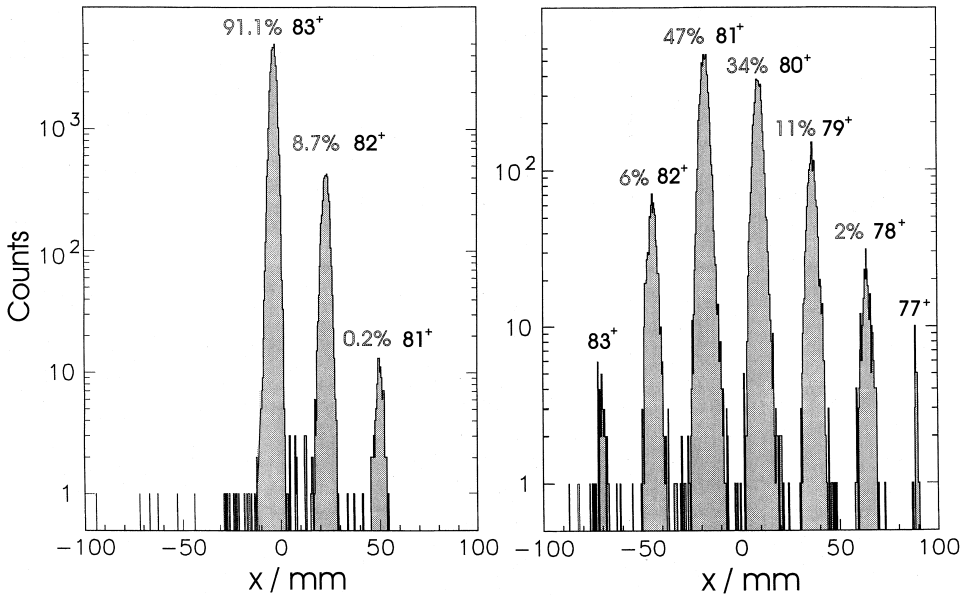

Fig. 2. Measured equilibrium charge-state distribution of ^{209}Bi projectiles in lead at 950 MeV/u (left panel) and 159 MeV/u (right panel). The number of counts is plotted versus the position coordinate (x) in the dispersive plane.

targets which were completely commercially treated and were characterized by chemical contaminants of the order of 1.2%, however as the contaminants are elements close to Be, therefore, the stopping power correction is negligible. The error of the target thickness determination is for most targets the dominant contribution to the overall error for the stopping powers which amounts to about 1%.

In general, the stopping power is defined as the mean energy loss per unit thickness, in the limit of infinitely small thickness, averaged over all particles. Practically all accelerator-based experiments provide projectiles in a fixed ionic state which can be far off the equilibrium mean charge state in the relevant stopping power target. At low energies in the MeV/u regime such effects are negligible since the target thickness to reach charge-state equilibrium is only a few μg/cm^2 or less. However, at relativistic energies the situation is different because the target thickness to reach charge-state equilibrium is much larger, e.g., it is 660 and 40 mg/cm^2 for 1000 MeV/u gold projectiles in beryllium and lead material, respectively. As mentioned above, the charge states of the extracted SIS beams correspond to the atomic interactions with stripper targets at much lower energies in the UNILAC, e.g., lead and bismuth projectiles have the charge state 67^+ emerging from SIS at all selected energies. A consequence is that the projectile would penetrate the first part of the stopping power target in a non-equilibrated CSD with a result of systematically lower measured stopping power. We avoided this influence by using an additional stripper target directly in front of our dE/dX-targets, i.e., the projectiles entered already the dE/dX-targets in a CSD close to equilibrium. Furthermore, the targets were chosen sufficiently thick such that the measured energy-loss of the projectiles after penetration of the target is to a very good approximation independent of the selected charge state for the Bρ analysis with the FRS.

2.3. Energy-loss straggling

The energy-straggling experiments require in principle the same preparations as described for the stopping-power measurements but in addition a high ion-optical resolving power and higher quality targets with respect to thickness inhomo-

genity are necessary. The high resolving power of the FRS is demonstrated in Fig. 3 with displayed position spectra corresponding to the measurements with and without the straggling target inserted in the beam. The energy straggling of relativistic heavy ions is relatively small and therefore difficult to measure. Already a contribution of thickness variations of the order of a few 10^{-3} can completely mask the energy-loss straggling due to the statistical fluctuations in the atomic collision processes. Therefore, we used carefully investigated and selected targets, which were characterized by a surface roughness in the range of 50–150 nm (rms value) [16] measured via laser interferometry at the PTB in Braunschweig. In addition, a collimator of 0.3 mm diameter was placed in front of the targets [15]. Both measures aimed to reduce possible straggling contributions due to target thickness nonuniformities. Even for the thinnest targets, e.g. for 0.3 mm Cu or 0.2 mm Au with the biggest surface roughness of about 150 nm (rms) the resulting enlargement of the energy straggling is only about 10%. In all other cases the effect is in the range of 1% or even lower.

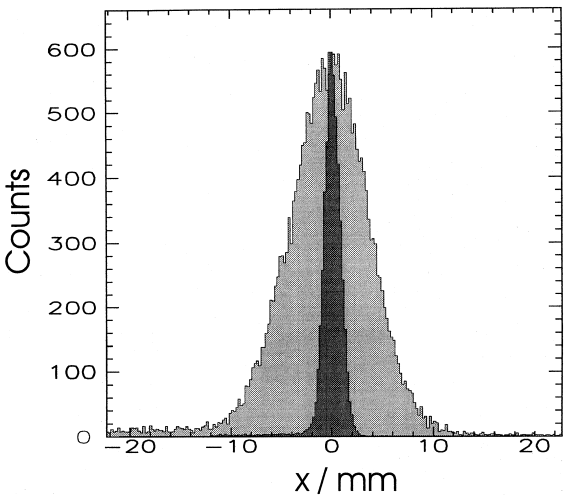

Fig. 3. Position spectra in the direction of the dispersion (x) corresponding to the measurements with and without the straggling target (Al 4 g/cm^2) inserted in the 1000 MeV/u ^{209}Bi beam. The maximum of the distribution without target is normalized to the one with the straggling target inserted.

3. Results

3.1. Charge states

The charge states of heavy ions penetrating matter are determined by the probabilities for electron capture and ionization collisions. Electron capture can occur via three different mechanisms: radiative electron capture (REC), non-radiative capture (NRC), and resonant transfer and excitation (RTE). These charge-changing processes have drastically different projectile, target and energy dependences [20,22]. In Fig. 4 we present new data of total electron capture cross-sections for bare, H-like and He-like ^{209}Bi projectiles in different target materials at 200 MeV/u. The results are compared with the theoretical predictions implemented in the computer program GLOBAL [20]. These theoretical predictions reproduce the Z_2-dependence of the experimental electron capture cross-sections well whereas the agreement of the absolute values is better for bare ions than for the H-like and He-like initial charge states.

The experimental results for the ionization of 200 MeV/u H-like and He-like ^{209}Bi projectiles are presented in Fig. 5, where the measured ionization cross-sections in different solids are compared with

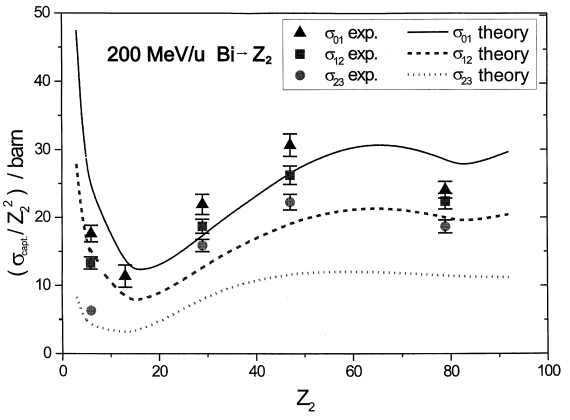

Fig. 4. Measured total electron capture cross-sections of bare, H-like and He-like ^{209}Bi projectiles in different solid target materials at 200 MeV/u. The data are compared with theoretical predictions implemented in the computer code GLOBAL [20,22]. σ_{ij} represents the charge-changing cross-section from the state with i bound electrons to one with j bound electrons.

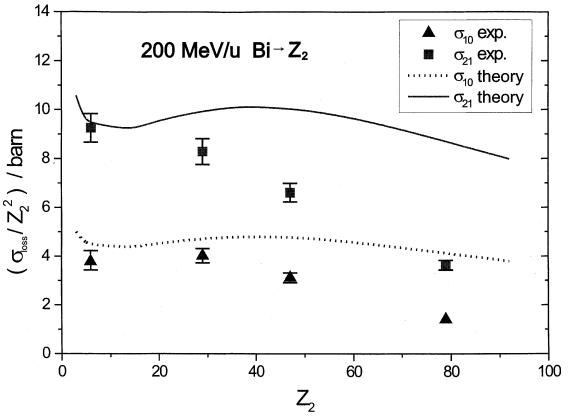

Fig. 5. Measured ionization cross-sections of He-like and Li-like ^{209}Bi projectiles in different solid target materials at 200 MeV/u. The data are compared with the theoretical predictions from the computer code GLOBAL [20,22]. σ_{ij} represents the charge-changing cross-section from the state with i bound electrons to one with j bound electrons.

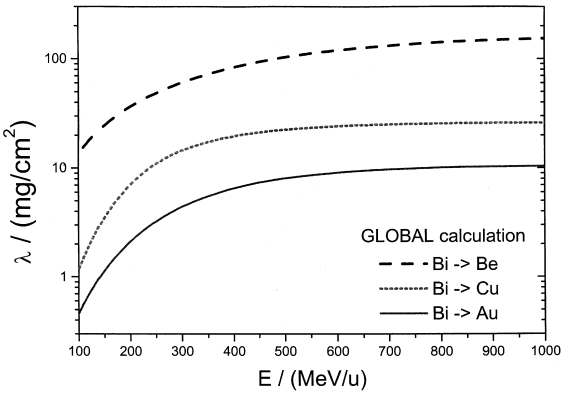

Fig. 6. Calculated mean free path lengths for charge change of H-like ^{209}Bi projectiles in Be, Cu and Au materials [20].

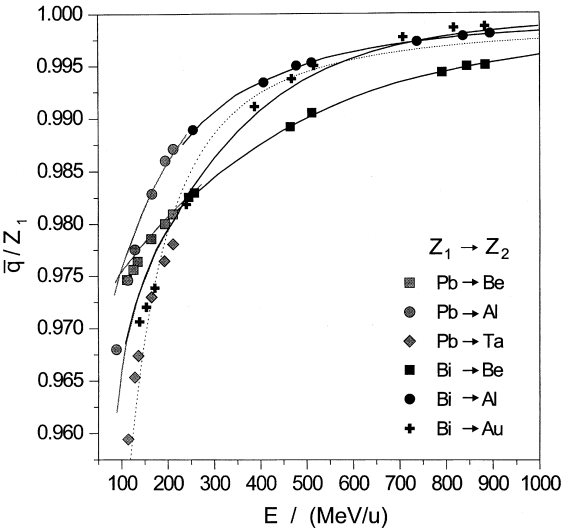

Fig. 7. Measured mean charge states of ^{208}Pb and ^{209}Bi projectiles in different target materials are compared with the corresponding predictions from GLOBAL (full lines) and an empirical charge parametrisation [17] (dashed line) in the energy range between 100 and 1000 MeV/u. The experimental errors are within the size of the symbols and the projectile-target combinations are indicated in the legend.

the theoretical prediction from GLOBAL [20,22]. The measured ionization cross sections are up to a factor of two lower than the theory [20], particularly for the high Z_2 targets. Both experimental results can be used to improve further the theoretical descriptions, which agree better for our earlier investigations at higher energies up to 1000 MeV/u [20,21].

Knowing the CCCS, one can calculate the mean free path length for charge-changing collisions, a quantity which is needed to simulate the ion penetration. The mean free path lengths for charge change of H-like ^{209}Bi projectiles are calculated with GLOBAL [20] and illustrated for Be, Cu and Au material in Fig. 6. It is clearly demonstrated that the mean free path lengths for charge change are the largest for the low-Z media in the energy range of 100–1000 MeV/u.

With increasing number of atomic collisions a charge-state equilibrium is reached in Fig. 7. The measured equilibrium mean charge states of ^{209}Bi projectiles in Be, Al, Ta and Au targets are compared with the corresponding predictions from GLOBAL and a simple empirical charge parametrisation in the energy range between 100 and 1000 MeV/u. It is observed that the simple mean charge relation [17] can also give a good first approximation although the lack is that the dependence on the stopping medium is not included. This formula for the effective charge (q_{eff}) is [17]

$$q_{\text{eff}} = Z_1\left[1 - \exp\left(\frac{-0.95\ v}{Z_1^{2/3} v_0}\right)\right], \qquad (1)$$

where v/v_0 is the projectile velocity in units of the Bohr velocity.

3.2. Stopping powers

A new theory on stopping of bare heavy ions up to ultra-relativistic energies has been developed by Lindhard and Sørensen [6] based on the Dirac equation. It also takes into account the deviation from a point-charge in case the de Broglie wave length of the scattered electron approaches the size of the projectile nucleus [30]. Our measured results for bare projectiles can be well described by the LS theory [32,26]. It is now of great interest how well the agreement holds down to lower energies where the heavy ions are no longer completely stripped. This question is addressed in a comparison in Fig. 8 where our measured stopping power values for ^{197}Au, ^{208}Pb and ^{209}Bi projectiles in different solid materials are plotted as a ratio with the corresponding LS values. The agreement with the approximation of bare nuclei in the theory is remarkably good down to 500 MeV/u, however, for lower energies it is clearly demonstrated that the lower projectile charge states have to be taken into account for a more realistic comparison. The observed deviations at 100 MeV/u, corresponding to 43% of the speed of light, amount to more than 9%.

A further step towards a more realistic comparison between theory and our data is depicted in Fig. 9. The LS theory is mainly adapted in two points: Firstly, Z_1 is replaced by q_{eff} using Eq. (1) which takes into account that the projectiles travel through matter with several electrons attached. Secondly, corrections like shell effects (up to 2% in lead at the lowest energy) [23] and a Barkas term (up to 5% in lead at the lowest energy) [24,25] have been included, for more details see [32]. In principle, the agreement is improved but it is also clearly demonstrated that an effective charge formula which does not take into account the Z_2-dependence yields systematic deviations up to 5%.

The next step towards an improvement was to insert into the theoretical description the partial stopping power values $(\mathrm{d}E/\mathrm{d}X(q_i))$ using the weights (w_i) for each charge state (q_i) from our measured equilibrium charge-state distributions:

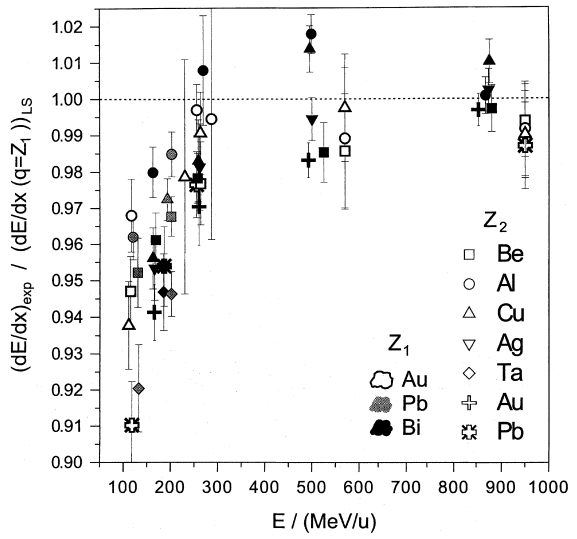

Fig. 8. Experimental stopping powers for ^{197}Au, ^{208}Pb and ^{209}Bi projectiles in different solid targets normalized by the corresponding values of the LS theory [6]. In the theory it is assumed that the projectiles are completely stripped. The projectile-target combinations are indicated in the legend.

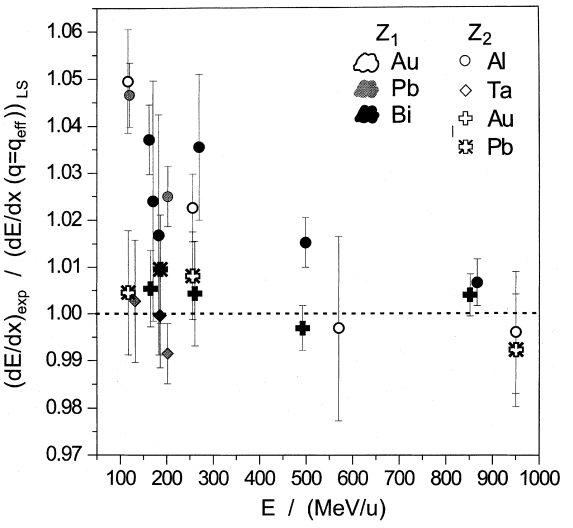

Fig. 9. Experimental stopping powers for ^{197}Au, ^{208}Pb and ^{209}Bi projectiles in different solid targets normalized by the corresponding values of LS theory [6]. In the LS theory the nuclear charge Z_1 is replaced by an effective charge [17].

$$\frac{dE}{dX} = \sum_i w_i \frac{dE}{dX}(q_i). \quad (2)$$

This model is certainly a better approximation which combines the knowledge of the CSD with the stopping power theory. Possible screening corrections represent a minor contribution for our relativistic projectiles, as can be deduced from theoretical investigations [18,19]. Indeed, as demonstrated in Fig. 10 the deviation between data and theory is now within the experimental error of about 1% with a slight systematic shift.

In summary, we have shown that the stopping power for bare and few-electron relativistic heavy ions can be well reproduced by the LS theory, especially if the experimental knowledge of the charge-state population is incorporated.

3.3. Energy-loss straggling

When ions penetrate matter, the statistical fluctuations of the impact parameters as well as the variation of the transferred momenta in the scattering events cause the width of the energy-loss distribution. At relativistic energies the energy straggling is mainly determined by close collisions of the heavy ions with the target electrons. In previous publications [5,32,26] we have shown that the energy straggling of bare heavy ions systematically deviates by a factor of up to 3 from the well-known theoretical descriptions based on first-order perturbation [1,27]:

$$\Omega^2 = 4\pi Z_1^2 e^4 N Z_2 \Delta X \left(\frac{1 - \beta^2/2}{1 - \beta^2} \right), \quad (3)$$

where $NZ_2\Delta X$ is the number of electrons per unit area and β is the projectile velocity in units of the speed of light. Those experimental results, however, were in good agreement with the predictions from LS theory [6]. In the Bohr and LS theories it is assumed that the heavy ions are completely stripped.

In this contribution, we present new energy-straggling measurements in different target materials with the goal to demonstrate unambiguously the role of the charge-exchange straggling in solid targets. At relativistic velocities we have the unique possibility to select the target material such that either the collisional straggling in a fixed charge state or the charge-exchange straggling is the dominant contribution. This statement can already be deduced from the presentation of the drastically different mean free path lengths for low- and high-Z solids presented in Fig. 6.

In our straggling measurements, the projectiles lost about 10–30% of the incident energy (E_0) in the targets used. A comparison with theoretical results requires that the energy dependence inside the targets is taken into account. This was done by numerical integration according to the formula

$$\Omega^2_{\text{target}} = \left(\frac{dE(E_1)}{dX} \right)^2 \int_{E_0}^{E_1} \frac{d\Omega^2(E')/d(\Delta X)}{[dE(E')/dX]^3} dE', \quad (4)$$

where E_1 represents the energy of the beam after penetration of the straggling targets.

In Fig. 11 we present new data on energy straggling of ^{209}Bi projectiles in different solid materials at 1000 MeV/u incident energy. The

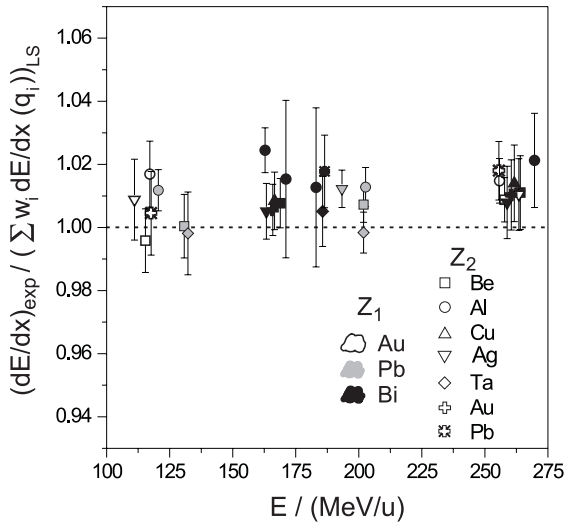

Fig. 10. Experimental stopping powers for ^{197}Au, ^{208}Pb and ^{209}Bi projectiles in different solids normalized by the corresponding values from theory. The theoretical stopping powers are given by a sum of LS stopping powers for $Z_1 = q_i$, weighted by the measured population of the charge states q_i.

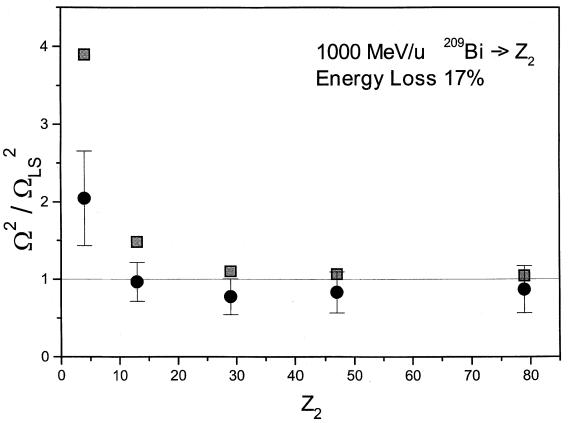

Fig. 11. Experimental energy-straggling values (full circles) of ^{209}Bi projectiles in different solid target materials compared to a Monte Carlo simulation (squares), both normalized by LS theory. The incident energy was 1000 MeV/u and the mean energy loss 17%.

results are compared to the predictions of the LS theory [6], and with results from a Monte Carlo simulation. In the Monte Carlo code the theoretical probabilities for charge-changing collisions were implemented in the form of statistically selected free path lengths and the slowing down was taken from the LS theory. The process simulated with the Monte Carlo program can also be treated fully analytically as it has been done by Sigmund [31]. This was applied for three charge states and lead to the same result. From these formulas it can also be seen that for a sufficiently thick target the variance of the charge-exchange straggling is inversely proportional to the charge-changing cross-sections.

The comparison of the results at 1000 MeV/u clearly demonstrates that we obtain excellent agreement with the LS theory for heavier target materials, whereas we observe strong deviations for beryllium. In the LS theory it is assumed that the projectiles are completely stripped. It is obvious to conclude that the contribution due to charge exchange straggling is the reason for the observed deviation. The Monte Carlo simulation can reproduce the heavier Z_2-material very well and indicates a transition to larger straggling values for the lighter target materials. However, before we want to conclude we present data at our lowest incident energy, where the charge-changing collisions should represent a more significant part.

The energy-straggling results of ^{209}Bi projectiles in different solid materials and target thicknesses at 200 MeV/u incident energy are presented in Fig. 12. The results are compared with the LS theory, where the effective charge states of Eq. (1) replace the assumption of bare ions. This modification is necessary at low energies as already illustrated in Fig. 8. The experimental energy straggling results show systematic deviations from the LS theory. At this energy also for the heavy target materials an energy straggling contribution is missing in the theory and for the light media (Be, Al) the theoretical results underestimate the measured data by a factor of about 6. As already mentioned we carefully avoided experimental systematic errors by going from light to heavy targets. Therefore, we conclude that the statistics of collision processes (see also Fig. 6) are different in low- and high-Z targets, i.e., the observed deviation is a direct consequence of the contribution of charge-changing collisions. To further prove this statement we employed our Monte Carlo simulation. The results of the simulation are in excellent agreement with the experimental data over the entire Z_2 range, a confirmation that indeed the charge-changing processes can explain the observations.

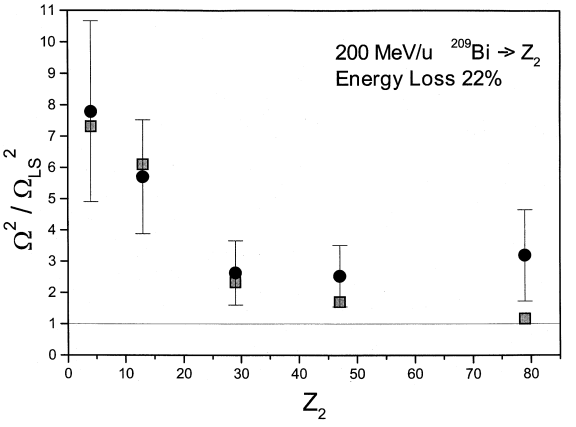

Fig. 12. Experimental energy straggling values (full circles) of ^{209}Bi projectiles in different solid targets compared to a Monte Carlo simulation (squares), both normalized by LS theory. The incident energy was 200 MeV/u and the mean energy loss 22%.

This is the first time that the contribution of charge-changing collisions to heavy ion energy straggling in solids can be explicitly experimentally demonstrated. At lower energies in the MeV/u region the interpretation of early measurements with heavy ions in amorphous solids was severely influenced by the target thickness variations. Therefore, the measurements were carried out only in gases, however, the clear separation of the different straggling contributions was experimentally not possible in this energy range [28]. Investigations on this subject at 17.6 MeV/u have also been performed in earlier channeling measurements [29].

In future experiments, we will continue to investigate the influence of charge-exchange straggling at different energies and for different projectiles. The large contribution of heavy-ion energy straggling due to charge-changing collisions has also strong influence on many applications with heavy-ion beams, e.g., it will decrease the resolution in energy deposition detectors, decrease the resolving power for the separation of monoenergetic exotic nuclei [8] and finally also widen the range distribution for implanted heavy ions.

4. New applications

Atomic interaction of heavy ions within ion-optical systems can be employed in many fields of research and applications [33,26]. Relativistic heavy-ion collisions with free electrons are the basis of a new generation of experiments which have been pioneered in the storage ring ESR [34] at GSI. The ions interact with a merged cold electron beam, in this way, the momentum spread has been reduced below 10^{-6} for low intensity heavy-ion beams and the transverse emittance of the circulating beam is less than 0.05π mm mr. These kinematical properties are ideally suited, e.g., for channeling experiments with high-energy heavy ions [35,36]. Such precision experiments with stored and cooled beams are not restricted to stable projectiles but have been extended to exotic nuclei [37–39].

The synchrotron SIS can provide heavy-ion beams with ranges of more than 30 cm in water. This gives the opportunity to use the heavy ions for biomedical applications, e.g. for tumor treatment [7] which has been successfully applied to patients recently at GSI. In the case of tumor treatment, the characteristic dose distribution and the favorable range and angular straggling of heavy ions are employed.

Applications relying on an extremely narrow range profile of relativistic heavy ions can use decelerated cooled beams extracted from the storage ring. The resulting narrow range profiles are required if the beam has to be completely stopped in a gas cell of a small lateral dimension. Unfortunately, the deceleration-cooling techniques cannot be applied for short-lived exotic nuclei since the deceleration by RF cavities in combination with electron cooling presently needs at least several seconds. The fastest method to transfer a relativistic beam to thermal velocities is the atomic slowing down in matter. This process takes place in the subnanosecond time interval. The electric field in the atomic slowing-down process is many orders of magnitude larger than that of the strongest electro-magnetic devices.

In a good approximation the range (R) and the range straggling of heavy ions in matter can be calculated within the continuous slowing down approximation:

$$R(E) = \int_{E_{\min}}^{E} (\mathrm{d}E/\mathrm{d}X)^{-1}\,\mathrm{d}E. \tag{5}$$

In principle, the narrowest range distribution can be obtained from an ideal monoenergetic incident beam. However, if the slowing down is done within a dispersive ion-optical spectrometer this limit can be elegantly overcome. The method is to perform a substantial part of the slowing down at the object plane of the spectrometer and bunch the resulting energy spread with an adequately shaped degrader (monoenergetic degrader) at the dispersive focal plane, see Fig. 13. Such a monoenergetic degrader exactly compensates the momentum spread of a spatially dispersed beam by larger or smaller energy losses, i.e., after passage of this degrader all ions have the same momentum. Depending on the thickness of the matter placed in the object plane the range straggling can be

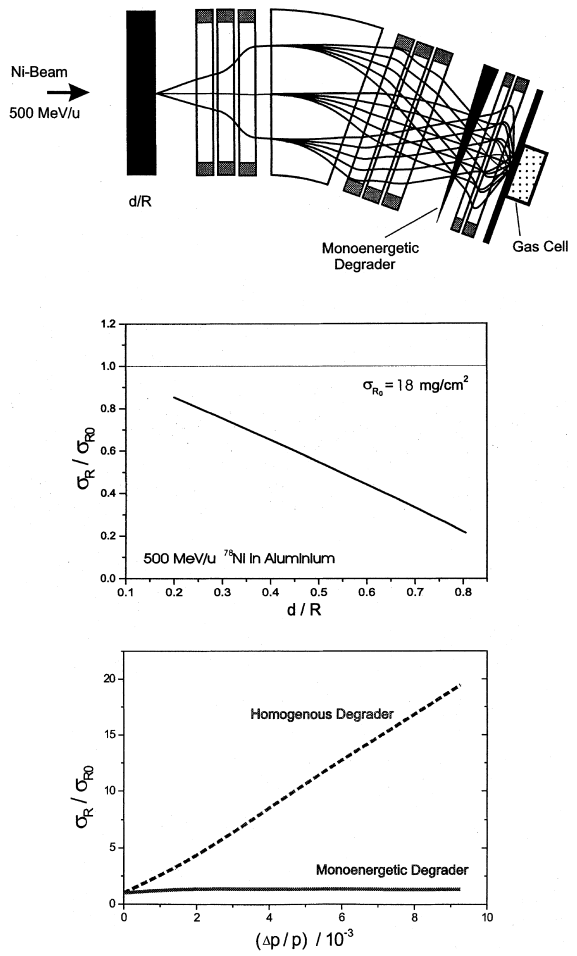

Fig. 13. Upper panel: Bunching of the range distribution of relativistic heavy ions by using the performance of a magnetic spectrometer. Central panel: Calculated illustration of range bunching for 500 MeV/u Ni projectiles below the range straggling of a monoenergetic beam [40]. σ_R/σ_{R_0} represents the range straggling normalized by the corresponding distribution of an incident monoenergetic beam. The thickness of the absorber, d/R, is given in units of the range of the incident projectiles. Lower panel: Range bunching of 500 MeV/u ^{78}Ni fragments in aluminum as function of the incident momentum spread.

reduced below the corresponding one of the incident monoenergetic beam. Using this technique, relativistic beams of exotic nuclei can be implanted in relatively small gas cells. This method was discussed in the international NUPECC meeting at GSI [40] and it was demonstrated that a gas-filled trap behind the FRS can be realized and will open new experimental prospects with exotic nuclei. Trapping of a beam of monoisotopic exotic nuclei represents excellent experimental conditions for LASER spectroscopy and decay studies in general.

The calculated range straggling for 500 MeV/u nickel projectiles in aluminum is presented as an example in Fig. 13. Before the beam is stopped in the gas cell the major part of the atomic range is spent in a suitable solid degrader optimized for small nuclear reaction rates and minimum atomic straggling contributions.

In case of relativistic exotic nuclear beams [8], the nuclear reaction kinematics of the production processes lead to an inevitable energy straggling which normally would cause a strong increase in the range straggling for implantation experiments. The application of a monoenergetic degrader placed in a spectrometer, as presented above, reduces the range straggling to a value close to that of an ideal monoenergetic beam. The range bunching of 500 MeV/u ^{78}Ni fragments in aluminum as a function of the incident momentum spread ($\Delta p/p$) is depicted in the lower part of Fig. 13 [40].

Presently, it is also discussed in different laboratories worldwide to combine a projectile fragment separator like the FRS with a gas cell where the range-bunched monoisotopic exotic beams are completely stopped [41]. Such an arrangement would elegantly allow to combine an in-flight facility for exotic nuclei with the coventional ISOL-technique for postaccelerated exotic nuclear beam experiments [8]. The scenario is again an example of a versatile application of the knowledge of slowing down of ions in matter.

References

[1] N. Bohr, Dan. Mat. Fys. Medd. 18 (8) (1948).
[2] S.P. Ahlen, Rev. Mod. Phys. 52 (1980) 121.
[3] P. Sigmund, Nucl. Instr. and Meth. B 135 (1998) 1.
[4] C. Scheidenberger, et al., Phys. Rev. Lett. 73 (1994) 50.
[5] C. Scheidenberger, et al., Phys. Rev. Lett. 77 (1996) 3987.
[6] J. Lindhard, A.H. Sørensen, Phys. Rev. A 53 (1996) 2443.
[7] G. Kraft et al., Proceedings of the EULIMA Workshop, Nice, 1988.
[8] H. Geissel, G. Münzenberg, K. Riisager, Ann. Rev. Nucl. Part. Sci. 45 (1995) 163.

[9] K. Blasche, B. Franczak, in: H. Henke, H. Homeyer, Ch. Petit-Jean-Genaz (Eds.), Proceedings of the Third European Part. Acc. Conf., Berlin, 9, Editions Fronitière, Gif-sur-Yvette, 1992.
[10] M. Steck et al., in: Proceedings of the Fifth European Part. Acc. Conf., 1996, p. 1185.
[11] H. Geissel, et al., Nucl. Instr. and Meth. B 70 (1992) 286.
[12] V. Hlinka, et al., Nucl. Instr. and Meth. A 419 (1998) 503.
[13] M. Pfützner, et al., Nucl. Instr. and Meth. B 86 (1994) 213.
[14] H. Folger, et al., Nucl. Instr. and Meth. A 303 (1991) 24.
[15] Th. Schwab, et al., Nucl. Instr. and Meth. B 48 (1990) 69.
[16] R. Krüger-Sehm et al., Laser interferometry measurements at the PTB in Braunschweig, 1999.
[17] T.E. Pierce, M. Blann, Phys. Rev. 173 (1968) 390.
[18] P. Sigmund, Phys. Rev. A 56 (1997) 3781.
[19] W. Brandt, M. Kitagawa, Phys. Rev. B 25 (1982) 5631.
[20] C. Scheidenberger, et al., Nucl. Instr. and Meth. B 142 (1998) 441.
[21] Th. Stöhlker, et al., Phys. Rev. A 51 (1995) 2098.
[22] J. Eichler, W.E. Meyerhof, Relativistic Atomic Collisions, Academic Press, New York, 1995.
[23] W.H. Barkas, M.J. Berger, NASA Report SP-3013, 1964.
[24] J.D. Jackson, R.L. McCarthy, Phys. Rev. B 6 (1972) 4131.
[25] J. Lindhard, Nucl. Instr. and Meth. 132 (1976) 1.
[26] H. Geissel, C. Scheidenberger, Nucl. Instr. and Meth. B 136 (1998) 114.
[27] M.S. Livingston, H.A. Bethe, Rev. Mod. Phys. 9 (1937) 245.
[28] H. Geissel, in: J. Bang, J. de Boer (Eds.), Semiclassical Descriptions of Atomic and Nuclear Collisions, North-Holland, Amsterdam, 1985, p. 431.
[29] J.U. Andersen, et al., Nucl. Instr. and Meth. B 90 (1994) 104.
[30] S. Datz, et al., Phys. Rev. Lett. 77 (1996) 113.
[31] P. Sigmund, Nucl. Instr. and Meth. B 69 (1992) 113.
[32] C. Scheidenberger, H. Geissel, Nucl. Instr. and Meth. B 135 (1998) 25.
[33] H. Geissel, et al., Nucl. Instr. and Meth. A 282 (1989) 247.
[34] B. Franzke, et al., Nucl. Instr. and Meth. B 24/25 (1987) 18.
[35] H. Geissel, Nucl. Instr. and Meth. B 67 (1992) 120.
[36] Y.L. Pivovarov, et al., Nucl. Instr. and Meth. B 119 (1996) 283.
[37] H. Geissel, et al., Phys. Rev. Lett. 68 (1992) 3412.
[38] H. Geissel, et al., Nucl. Instr. and Meth. B 126 (1997) 351.
[39] H. Geissel et al., in: B.M. Sherrill, D.J. Morrissey, C.N. Davids (Eds.), AIP Conference Proceedings, Vol. 455, 1998, p. 11.
[40] H. Geissel, C. Scheidenberger, in: Proceedings of the International NUPECC Meeting held at GSI, December 1998.
[41] H. Grander, B.M. Sherrill, J. Nolen et al., ISOL Task Force Report to NSAC, 1999, http://srfsrv.jlab.orglisol.